Local Wind Speed Estimation by Physical Downscaling of Weather model forecasts

J. W. Verkaik *, A. J. M. Jacobs, A. B. C. Tijm, J. R. A. Onvlee

Royal Netherlands Meteorological Institute (KNMI), De Bilt, the Netherlands

Abstract

Wind speed forecasts by numerical weather prediction (NWP) models in heterogeneous terrain lack local representativity as they are derived using grid-box averaged roughness lengths. In this paper a downscaling method is presented to increase the local accuracy of NWP-wind speed forecasts.

The method includes a simple two-layer model of the atmospheric boundary layer, used in combination with a high-resolution roughness map. The 2L-model is used to post-process direct NWP-model output. The model comprises a surface layer and an Ekman-layer. In the surface layer vertical wind speed transformations are done using the logarithmic wind speed profile. In the Ekman-layer geostrophic resistance laws are applied.

The roughness map is derived from a land-use map and a simple footprint model. The roughness lengths are wind direction dependent and the footprint area of the Ekman-layer extends farther upstream than that of the surface layer. The roughness lengths compare well to those derived from gustiness analysis for station locations. The adjustment of the surface wind after a roughness transition as modeled by the two-layer model is similar to that of internal boundary layer models.

The NWP-model wind and the downscaled wind are evaluated in coastal zone areas, in estuaries, and at an airport in the Netherlands. Verification against in-situ observations shows that the downscaling method reduces the NWP surface wind speed error significantly, largely in terms of bias. The quality of the downscaled wind, however, depends highly on the quality of the high-resolution roughness map: inaccuracies of the land-use map may lead to local errors in the downscaled wind.

Key words: wind, roughness, local wind speed estimation, downscaling

* Corresponding author. Tel: +31 30 2206 864. Fax: +31 30 2204 614
Email address: job.verkaik@knmi.nl (J. W. Verkaik).

1 Introduction

Detailed near-surface wind speed forecasts are of vital importance to many public sectors and industries such as aviation, wind energy, navigation and water management. Managing operations in these fields requires wind information with a high level of spatial detail (< 1 km). Most numerical weather prediction models provide information on spatial scales varying from 10 to 40 km. On scales smaller than the NWP-model grid, spatial wind speed variations are caused mainly by differences in roughness and stability, with roughness effects dominating at higher wind speeds. Surface roughness often varies on horizontal scales much smaller than the NWP-model grid and consequently the NWP-model wind forecasts lack representativity. Nowadays high-resolution land-use data, based on satellite observations, are available on scales as little as tens of meters. This enables the addition of greater detail to NWP-model winds.

This paper presents a high-resolution wind transformation model (henceforth called the 2L-model), that produces locally representative near-surface wind forecasts with a horizontal grid spacing of 500 m. Such high resolution is beyond the limit of current operational mesoscale models. The basis of the 2L-model is the assumption that sub-grid-scale wind speed variations are caused mainly by surface roughness changes. These variations can be modeled by boundary layer theory on the condition that the relevant roughness parameters are known.

The 2L-model was first developed as an interpolation method for surface wind measurements (Wieringa, 1986; Verkaik and Smits, 2001). In the present study NWP-model forecasts provide the input wind speed, which are downscaled by the 2L-model. The 2L-model adjusts the wind speed of the NWP-model output, so the downscaled results have the same averaging timescales as the NWP-model.

The 2L-model is applied to derive detailed forecasts of wind fields in the Netherlands for the coastal waters in the province of Zeeland, and for the take-off and touch-down area at Amsterdam Airport Schiphol. The model is computationally very efficient which enables several Dutch authorities in the field of water management to run the 2L-model at their own computer systems and generate high-resolution wind data on customized grids as input to their warning systems and models for sea state, waves and currents. The NWP-model output they receive from the Royal Netherlands Meteorological Institute (KNMI). In this paper verification results of the downscaled wind are presented for those regions. We focus on the merits of the 2L-model, the verification of the NWP-model is beyond the scope of this paper.

Downscaling models for wind have been the subject of earlier studies. Recently De Rooy and Kok (2004, henceforth DR&K) presented a method in which they also used a high-resolution roughness map in combination with a physical downscaling model, to correct for the sub-grid-scale variation of the NWP-model output. In addition, they used a statistical correction to compensate for the grid-scale NWP-model error. For the part of the sub-grid-scale variation their method and the 2L-model are similar except that their model uses a local, but directionally constant, roughness parameter in the downscaling, while the 2L-model uses roughness parameters that depend on wind direction. The 2L-model is therefore better suited for areas with large roughness transitions. DR&K determine the NWP-model error in every grid box from wind speed observations. After the introduction of a new version of the NWP-model, DR&K need to determine the NWP-model errors again. The 2L-model, however, can be applied directly.

2 Two-layer model of the PBL

The objective of the 2L-model is to model the roughness induced wind speed differences at the surface. The relative magnitude of the wind speed variations decreases with height. While there may be large wind speed variations at the surface, at higher levels the wind speed will be much more horizontally homogeneous. The smaller the horizontal scale of the surface roughness heterogeneity, the lower the blending height, i.e. the height at which the wind speed variations blend into the mean flow. At the blending height the average wind speed can be assumed horizontally constant. This is the basis of many interpolation and downscaling techniques (Wieringa, 1986; Bergström et al., 1988; De Rooy, 1995; Hutjes, 1996). In the 2L-model the blending is achieved in two steps. We assume that the small-scale wind speed variations have blended at the top of the SL ($\approx$ 60 m height), and the large-scale variations at the top of the PBL ($\approx$ 0.5–1 km height). So, a small-scale, local roughness parameter is used in the SL and a regional roughness parameter is used in the EL.

The 2L-model is a simple 1-D boundary-layer model of the PBL in two layers. The lower layer is the surface-layer (SL) where Monin-Obukhov theory is used (Obukhov, 1971; Businger and Yaglom, 1971; Tennekes, 1973). In this layer there is a strong vertical gradient in wind speed. There is no change in wind direction. The neutral version of the logarithmic wind speed profile is used to express the increase in wind speed U [m s^{-1}] with height z [m] :

$$U(z) = \frac{u_*^l}{\kappa} \ln \frac{z}{z_0^l}. \tag{1}$$

Here the Von Kármán constant $\kappa = 0.4$ (Frenzen and Vogel, 1995a,b), and

u_*^l [m s^{-1}] is the local friction velocity. The friction velocity is a measure for momentum transfer at the surface by friction: $\tau = \rho u_*^2 = -\rho\overline{u'w'}$. Here τ is the surface tension, ρ is the density of air, and $\overline{u'w'}$ is the covariance of the turbulent fluctuations of the longitudinal and vertical components of the wind speed. The roughness length used in this layer is the local roughness length z_0^l [m].

In the second layer, the wind speed increases further and in addition the wind direction veers (turns clockwise) in the northern hemisphere. Following Brown (1982) and Garratt (1992) we will call this layer the Ekman-layer (EL). This is described by the introduction of a second wind speed component, perpendicular to the surface wind speed. The geostrophic resistance laws are applied to relate the wind speed at the top of the PBL to the friction velocity (Garratt, 1992, cf. chapter 3):

$$\begin{aligned} U_{\text{macro}} &= \frac{u_*^r}{\kappa}\left[\ln\frac{h}{z_0^r} - A\right], \\ V_{\text{macro}} &= -\frac{u_*^r}{\kappa}\text{sgn}\,(f)\,B. \end{aligned} \tag{2}$$

U_{macro} and V_{macro} are the components of the wind speed at the top of the EL, the macrowind. U_{macro} is parallel to the surface wind, V_{macro} is perpendicular to U_{macro}. With U_{macro} in eastward direction, V_{macro} points northward in the northern hemisphere. The Coriolis parameter f [s^{-1}] equals $2\Omega\sin\phi = 1.1 \cdot 10^{-4}$ Hz at latitude 52° North, where Ω is the angular velocity of the Earth's rotation and ϕ is the latitude. The roughness length used in this layer is the regional roughness length z_0^r, h is the PBL-height. For A and B the values for neutral stability of the parameterization by Arya (1977) are adopted: $A = 1.9$ and $B = 4.5$. For neutral boundary-layers an alternative formulation for Eq. 2 is available in which the PBL-height is no longer required as external parameter. We prefer to use Eq. 2, which is the neutral limit of the non-neutral form of the geostrophic resistance laws, including the PBL-height. Comparison of downscaled wind speeds with measurements showed that this approach performs better than using the neutral formulation without the PBL-height.

The downscaling of NWP-winds using the 2L-model goes as follows (see Fig. 1). The friction velocity u_* is computed from the 10-m wind and the NWP-model roughness using Eq. 1. Next the wind speed at the top of the EL is computed from Eq. 2. The wind speed at the top of the EL is interpolated bi-linearly to the target location. At the target location the wind speed at the top of the SL is then computed from Eq. 2 and the regional roughness of the target location, and then the surface wind speed at the target location is computed using Eq. 1 and the local roughness.

The 2L-model is used assuming neutral atmospheric stability. This may seem to be a severe limitation of the applicability of the 2L-model but it is not: as

will be shown the error in the wind speed estimate that enters in the upward transformation from the negligence of stability effects is counterbalanced in the downward transformation (De Rooy and Kok, 2002). For this reason the 2L-model can be used for the interpolation of climatological wind fields when data on local stability is often not available.

In the present application the input wind speed is provided by the NWP-model. Besides the surface wind speed, the NWP-model provides wind speed at elevated levels as well as information on PBL-height and stability (Vogelezang and Holtslag, 1996). So if the 2L-model is used in combination with a NWP-model, it is possible to bypass the upward transformation at the input grid and start with the mathematical interpolation of the NWP-model wind at PBL-height level. The counterbalancing stability effect is then negated and the geostrophic resistance laws and the logarithmic wind speed profile must be used including stability corrections. In this paper we will show that this approach was not successful. The main reason for this failure is the problems we had with the determination of an accurate stability parameter from the NWP-model in stable conditions. The geostrophic resistance laws and the logarithmic wind speed profile require the Obukhov length stability parameter (L). In the NWP-model L is not used. It has to be deduced from the wind speed and temperature gradients between model layers. However, we have not succeeded in finding a method that yields an appropriate value for L for all weather types. Moreover, the NWP-model we used was known for having a problem modeling stable boundary layers, too strong vertical mixing, which has been a common problem to many NWP-models. Therefore, in the present application of the 2L-model we will use the NWP-model surface wind as input and will apply the neutral version of the geostrophic resistance laws and the logarithmic wind speed profile.

In barotropic situations the macrowind approximates the geostrophic wind, i.e. the wind is parallel to the isobars. In baroclinic conditions the macrowind may deviate from the geostrophic wind and the NWP-model wind at PBL may be quite different as well. As discussed, this is not relevant to the wind speed transformation. However, the direction of the macrowind is used to determine the footprint for the regional roughness. If the turning of the wind direction with height deviates significantly from that in neutral situations, for example in cases of strong cold advection, the direction of the footprint may be in error.

3 The roughness map

The 2L-model requires roughness lengths for the SL and EL. These are derived using a simple footprint model for a locally regular grid covering the Netherlands with a resolution of 500 m. Because of the detail of the land-use

map and the considerable size of the footprint, the evaluation of the roughness map is computationally very demanding. So the roughness map is not determined in run-time, but for every 500-m point in the domain the wind direction dependent roughness length is determined prior to running the downscaling method. The roughness caused by water, if present in the footprint, is treated separately since it has to be computed in run-time when the wind speed is available.

3.1 Spatial data on land-use

The roughness map is derived from the high-resolution land-use map LGN3+ [1] (De Wit et al., 1999). This map is a raster file covering the Netherlands with a resolution of 25 m. Every pixel in the map represents a typical land-use class. The accuracy, defined as the chance that the actual land-use is correctly classified in LGN3+, is over 90% for built-up areas and most nature areas. The reliability, defined as the chance that the correct land-use type is found at a pixel classified by that land-use, is over 90% as well for most land-use types in LGN3+.

To each of these land-use classes in LGN3+ we assigned a roughness length adopted from literature Wieringa (1993). In Table 1 the land-use classes and the assigned roughness lengths are listed. Two classes were added to LGN3+: airport runways and parking lots. This was done because in LGN3+ the concrete runways and airport platforms were included in the category "built-up area". During the evaluation of the roughness length in the vicinity of runways too high values were found. This proved to be especially troublesome in the validation of the downscaling method using measurements done at airports. This problem could be solved partially by correcting the land-use map. The runways were identified by hand and added to the new class with low roughness. The same applies to large parking lots in the Amsterdam Airport Schiphol area. However, the corrections applied to the land-use map of Schiphol are very crude and far from complete as yet.

No data on land-use in the neighboring countries Germany and Belgium are available to us at present. Therefore we do not use test stations close to the national border in this study. Neither did we include seasonal effects of canopy growth or deciduous trees dropping their leaves in winter on the roughness length.

[1] http://cgi.girs.wageningen-ur.nl/cgi/projects/lgn/

3.2 Surface elevation

In the major part of the Netherlands orography plays a minor role. However, in some areas orography does add to the total roughness and therefore it is taken into consideration. Surface elevation is assessed from the GTOPO30 [2] database. In this database the surface elevation is given at a resolution of $(1/120)^\circ$ (≈ 1 km). This grid has been interpolated using spline approximation techniques and exported into a new grid on a 500-m resolution in local (X, Y)-coordinates. Height differences are assessed by comparing the height at point (X, Y) with the neighboring points on the 500-m grid.

The roughness length due to orography $z_{0\mathrm{H}}$ is computed from

$$z_{0\mathrm{H}} = 0.2 \cdot \Delta H^2 / L, \tag{3}$$

where ΔH is the maximum height difference over distance L (Agterberg and Wieringa, 1989), here $L = 500$ m.

The resolution of GTOPO30 is not high enough to resolve small hills, dikes, etc. In the coming years a high-resolution elevation map of the Netherlands will become available. Then this part of the roughness map will need to be revised. It should also be noted that although orography adds to the roughness on large scales, on small scales orography may induce acceleration of wind and complex circulation patterns around hills (Jackson and Hunt, 1975; Jacobs, 1984). In the 2L-model these effects are not incorporated. So in cases where orographic forcing on the flow is not resolved by the NWP-model, the 2L-model will not solve this problem.

3.3 Area-averaged surface roughness

A suitable manner to aggregate surface roughness is to average the drag coefficients at the blending height (Wieringa, 1986; Mason, 1988; Claussen, 1990). This method gives stronger weight to the larger roughnesses in the averaging domain. The blending height is a function of the horizontal scale of the roughness fluctuations. Small-scale roughness fluctuations lead to a stronger enhancement of the effective roughness than large-scale fluctuations, although the roughness lengths and their areal fractions are equal (Schmid and Bünzli, 1995). We use a fixed blending height of 60 m at which the drag coefficients are averaged, following Wieringa (1986). This corresponds to the maximum SL-height. In areas with small-scale ($\lesssim 1$ km) roughness fluctuations this methods

[2] http://edcdaac.usgs.gov/gtopo30/gtopo30.html

slightly underestimates the effective roughness in comparison to other estimates (Baldauf and Fiedler, 2003). For the regional roughness, averaging can be done at a higher level. However, using a higher level does not lead to significantly different roughness values for the regional roughness. So we average the drag coefficients at 60-m height for the regional roughness as well.

The neutral drag coefficient is defined as $C_d \equiv (u_*/U)^2$ and assuming a neutral logarithmic wind speed profile (Eq. (1)) it can be expressed as

$$C_d = \left[\frac{\kappa}{\ln(z/z_0)}\right]^2. \tag{4}$$

The roughness due to orography can also be expressed as a drag coefficient using this equation. This orographic drag can be added to the 'skin drag'. Next, Eq. (4) can be inverted to compute the roughness length from the total drag.

3.4 Drag relation for water

The roughness of water is a strong function of wind speed. It also depends on wave age and water depth. Consequently, an average roughness length cannot be given independently of the wind speed. The roughness of the water in the footprint can therefore be determined only during runtime.

The total drag at the evaluation point for wind directions in sector j is computed from

$$C_d = C_{d,j} + f_{w,j} \cdot C_{water}(U), \tag{5}$$

where the drag of water can be expressed using Eq. (4) and the Charnock relation

$$z_0 = \alpha \cdot u_*^2/g, \tag{6}$$

where g is the acceleration of gravity [9.82 m s^{-1}] and for α the value 0.017 is used, which applies to long fetches over deep seas (Charnock, 1955; Garratt, 1977). For shallow waters, values as large as 0.032 have been reported for α (Onvlee, 1993; Benschop, 1996). In the NWP-model the value of 0.017 is used and we hold on to that value to prevent a bias in the downscaled wind speed over sea. Basically, α is determined by the wave conditions which in turn are a function of wind speed, water depth and wave age (Makin, 2003). The kinematic viscosity ($1.5 \cdot 10^{-5}$ m) is used as a lower limit to z_0.

Although wave growth is sensitive to the drag relation, for wind speed the exact form of the drag relation is less crucial. This is because the wind speed

always depends on z_0 in a logarithmic way: $U \propto \ln(z/z_0)$. For large values of z/z_0, U becomes a weak function of z_0.

4 Footprint model

During the advection of air parcels in the PBL by the flow, their physical properties are influenced by the surface properties. Consequently, meteorological parameters observed at a certain location will reflect the surface properties upstream of this location, the source area. The source area can be estimated from footprint models (Schmid, 1994; Horst and Weil, 1992; Horst, 1999). The footprint area for the average wind speed at a 10-m height over open terrain extends several hundred meters upwind. On shorter distances significant changes in the wind speed can be expected in the vicinity of obstacles. The flow around these obstacles, however, can not described the logarithmic wind speed profile.

In Fig. 2 an illustration of the footprint for two different measuring heights near a coastline is given. At some distance inland we imagine a measuring tower with sensors at two heights. The wind is onshore. The footprint of the lower sensor is small and is close to the tower. This is indicated by the ellipsoids at the surface, partially over land and partially over water. The inner ellipsoid could represent the area which determines 50% of the measured entity by this sensor, the outer ellipsoid represents the 90% area. All numbers and scale ratios in this example are fictitious.

4.1 Footprint approximation

Here we will make a simple approximation of the footprint using the following procedure. The area surrounding the evaluation point is split into 72 direction sectors each 5° wide. For each pixel i in sector j the drag coefficient at the blending height is determined from the equation

$$C_{d,i} = \left[\frac{\kappa}{\ln(z_{bh}/z_0)}\right]^2. \tag{7}$$

The roughness length is determined from Table 1. The drag coefficient of water is wind speed dependent and is not added to the total drag at this stage.

A weighted average of $C_{d,i}$ is computed using the weighting function

$$W(x_i, D) = \exp(-x_i/D), \tag{8}$$

where x_i is the distance from the source area to evaluation point, and D is a length scale determining the size of the footprint. We use 600 m for the local footprint, and 3 km for the regional footprint (see section 4.2). The average drag coefficient of sector j is given by

$$C'_{d,land,j} = \frac{\int_S \delta\,(\text{land})\, W\,(x_s, D)\, C_{d,s}\; ds}{\int_S W\,(x_s, D)\, ds}, \tag{9}$$

$$C'_{d,water,j} = \frac{\int_S \delta\,(\text{water})\, W\,(x_s, D)\, C_{water}\,(U)\, ds}{\int_S W\,(x_s, D)\, ds} = f'_{w,j} \cdot C_{water}\,(U)\,. \tag{10}$$

Here $\delta\,(\text{land})$ equals 1 if the considered pixel is covered by land and $\delta = 0$ otherwise. Similarly $\delta\,(\text{water}) = 1$ for water and 0 otherwise. $C_{water}\,(U)$ will be determined in runtime when U is available. $f'_{w,j}$ represents the weighted fraction of water in the footprint.

For practical reasons only the source area up to a distance of $3 \times D$ is considered. This corresponds to 80% of the total integral $\int_0^\infty \phi x \exp\,(-x/D)\, dx$ ($\phi x \cdot dx$ is the surface area at distance x, ϕ is the width of the sector in radians). Note that the relative surface contribution to the weighted sum reaches a maximum at distance D.

Now the direction dependent $C'_{d,j}$ and $f'_{w,j}$ are smoothed using a weighted moving average:

$$C_{d,j} = \sum_{k=-2}^{k=2} w_k \cdot C'_{d,j+k} \quad \text{and} \tag{11}$$

$$f_{w,j} = \sum_{k=-2}^{k=2} w_k \cdot f'_{w,j+k}, \tag{12}$$

where $w_{-2,-1,..+2} = \{0.08, 0.13, 0.18, 0.22, 0.18, 0.13, 0.08\}$. This bell shape has been chosen in accordance with sophisticated footprint models (Schmid, 1994).

4.2 Footprint length scales

Footprint length scales have to be selected for the regional and local roughness, D_r and D_l respectively. The footprint dimensions depend on roughness, measuring height, and stability (Horst and Weil, 1994; Schmid, 1994). The roughness map can not be assessed in run-time, so we use fixed values for D_r and D_l. Estimates for the footprint length scale can be made from the literature. It is also possible to validate the roughness lengths from the footprint model with estimates from other sources and adjust the footprint length scales to reach a satisfactory resemblance (section 4.3). The footprint length scales

determine the rate at which the surface wind speed will adjust to a new surface roughness after a roughness transition. So internal boundary-layer models may serve as a reference as well (section 4.4).

The wind speed profile up to height z will only in equilibrium with the local surface roughness if that roughness extends $100 \times z$ upstream (Bradley, 1968; Rao et al., 1974; Duijm, 1983). Fetches of more than 10 km are required before the SL is in complete equilibrium according to Taylor (1987). An estimate for the regional footprint length scale can be made from Schmid (1994, cf. figure 5h). It shows that with $O\left(z/z_0\right) = 10^2 \rightarrow O\left(D_\mathrm{l}/z_0\right) = 10^3 \ldots 10^4$ in near-neutral conditions. This implies that D_l will be several hundreds of meters. Most of the footprint estimates and fetch requirements apply to the SL only. Hardly any references are available for the regional footprint length scale or roughness length. Jensen (1978) argued that for the whole PBL to be in equilibrium, homogeneous fetches of several tens of kilometers are required. So D_r will be at least several kilometers, but a solid estimate is hard to establish.

4.3 Comparison with gustiness measurements

The roughness map can be verified by comparing the roughness length to that of other sources. The canonic way to determine the roughness length at a certain location is by determining the wind speed profile. Accurate instrumentation and careful interpretation is required to do so (Wieringa, 1980; Wyngaard et al., 1982; Horst, 1999). Assessment of the roughness length from profiles is therefore limited to specific research sites and it is unfeasible to analyze large areas this way. There are alternative methods, however, based on turbulence statistics from measurements at a single level (Sozzi et al., 1998). Gustiness analysis is one of these methods.

We will compare the local roughness length derived from the land-use map (z_0^l) to gustiness derived roughness lengths ($z_{0\mathrm{gust}}$) for the Dutch measuring station locations. These have been measured and analyzed at most Dutch wind stations since 1971 (Wieringa, 1976; Beljaars, 1987; Verkaik, 2000). The gustiness derived roughness is a function of wind direction and, if the station's environment changes, also a function of time. The difference in roughness length will be expressed as follows. The ratio (f_1) of the 60-m wind to the 10-m wind is computed from of Eq. (1) using $z_{0\mathrm{gust}}$:

$$f_1 = \ln(60/z_{0\mathrm{gust}}) \Big/ \ln(10/z_{0\mathrm{gust}}), \tag{13}$$

and the ratio f_2 is that of the 10-m wind to the 60-m wind using z_0^l from the roughness map:

$$f_2 = \ln(10/z_0^l) \Big/ \ln(60/z_0^l). \tag{14}$$

The error factor is

$$\text{Error factor} = f_1 \cdot f_2. \tag{15}$$

With a perfect match ($z_0^l = z_{0\text{gust}}$) the error factor equals 1.

The average error factor and its standard deviation have been determined for a range of values for D_l. Best results where found for $D_\text{l} = 0.6$ km. Then the average error factor is 1.023 with a standard deviation of 0.076.

In Fig. 3 the error factor is plotted for 34 stations for $D_\text{l} = 0.6$ km. For each station $z_{0\text{gust}}$ has been determined for recent years. It has been computed for 18 wind direction sectors of 20° wide. From this figure it can be seen that for sectors with a low $z_{0\text{gust}}$ the error is usually less than 10%. The cluster of points with high $z_{0\text{gust}}$'s comprises most of the onshore stations. In this cluster there is a slight trend of increasing error with increasing $z_{0\text{gust}}$. This implies that for large $z_{0\text{gust}}$'s, the z_0^l's tend to fall behind. Close examination of some obvious errors reveals that often the land-use map is in error in these cases. This is partially due to its finite resolution. With a pixel size of (25 m)^2 isolated obstacles may not be resolved. These obstacles can have a large impact on the observed gustiness and wind speed.

In the low $z_{0\text{gust}}$-sectors there is often water present in the footprint. The error factor in these sectors is more often larger than 1. This could be the result of our choice for $\alpha = 0.017$ in Eq. (6). This value must be considered as a minimum, and may need enhancement.

4.4 Comparison with internal boundary-layer models

The rate at which the surface wind speed adjusts to a new surface roughness in the 2L-model is described by D_l and D_r. Increasing D will increase the length of the fetch required to achieve a new equilibrium. This response rate can also be described by internal boundary-layer models (IBL-models). Here we will compare the development of the wind speed after a roughness change in the 2L-model to that of IBL-models. Most IBL-models have been developed for the SL only. However, there are IBL-models developed for the whole PBL as well. From these models a regional footprint length scale may be found.

We consider the sea–land transition (and vice versa) where the land rough-

ness length is 0.1 m. Beside the 2L-model we will use the IBL-models by Kudryavtsev et al. (2000, henceforth K2000), Troen and Petersen (1989, henceforth WASP), Van Wijk et al. (1990, henceforth COAST), and a surface-layer IBL-model by Townsend (1965). For the 2L-model and Townsend's model the roughness length of the sea is assumed to have a value of 0.001 m, the other models compute the drag of the sea from the wind speed. K2000 and COAST are used in near-neutral mode, the other models are neutral by themselves. A value of 10 m s^{-1} has been adopted for the wind at 10 m height over sea. The results are plotted in Fig. 4. The 2L-model is used with $D_l = 0.6$ km and $D_r = 3$ km. Fig. 4(a) shows the sea–land transition, Fig. 4(b) the land–sea transition where the wind speed over land is fixed at 7 m s^{-1}. COAST is developed for onshore flow only.

Apart from Townsend's model, all models show a similar adjustment of the 10-m wind to the new surface roughness for short fetches. The 10-m adjustment in the 2L-model compares well to the IBL-models. However, for short fetches the 2L-model adapts slower than most IBL-models. This suggest a smaller value to be used for D_l. For this study the map with $D_l = 0.6$ km was the only one available, however.

Although the development of the 10-m wind after a change in roughness in the 2L-model is similar to that of IBL-models, there are important conceptual differences between IBL-models and the 2L-model. Simple IBL-models give a formula for the IBL-height growth rate and an assumption on the wind speed profile in the disturbed layer. In terms of the 2L-model the footprint of the profile above the IBL-height lies entirely upstream of the roughness transition and the footprint of the profile below the IBL-height lies entirely downstream of the roughness transition. The interface of the two layers climbs with fetch. In the 2L-model the interface is fixed at the blending height while the roughness lengths are gradually adjusting.

Every change in surface roughness will cause internal boundary-layers to emerge, so their number may be large. IBL-models have difficulties handling many transitions and their validation in this context is also poor. Furthermore, IBL-models require a well defined sequence of roughness changes along a line upwind of the site of interest. This usually implies major simplifications to the roughness map.

4.5 Sample of the roughness map – Zeeland estuaries

In Fig. 5(a) the surface roughness map of the NWP-model is presented for the Zeeland area. The resolution of the roughness map is 0.1°. Note that the NWP-model roughness lengths are small in most parts of the Zeeland province,

even over land. In Fig. 5(b) the local roughness for the same area is plotted. The roughness of water is computed using homogeneous wind field (5 m s^{-1} south-southwest). In contrast to the NWP-model roughness map there are sharp gradients in the local roughness map along the coastlines and urban areas.

In Fig. 6 the regional NWP-model roughness length at location Hansweert (cf. Fig. 7) is compared to the direction dependent local and regional roughness lengths derived from the land-use map. For comparison, roughness lengths derived by gustiness analysis are presented as well. For winds over land (offshore) the local roughness lengths in the SL are in good agreement with the gustiness analysis. Note that for offshore winds (directions northwest to northeast) the NWP-model roughness is much too low. For onshore winds (directions southwest to southeast), where the roughness is dominated by the presence of at least 80% water, the NWP-model roughness is too high. Note also that the difference between $z_{0\text{gust}}$ and z_0^l for onshore winds indicates that for this location the footprint length scales are chosen too small.

5 NWP-model data

The NWP-model that is used in the verification study to provide the necessary input data is the operational mesoscale Hirlam model. Hirlam is a weather forecasting and data-assimilation system with all the necessary physics such as cloud physics, convection, a turbulence parameterization, a soil parameterization and radiation. It is developed by the international Hirlam project (Undén et al., 2002). This is a joint effort of Denmark, Iceland, Ireland, Finland, the Netherlands, Norway, Spain and Sweden.

Hirlam is a limited area model like ETA, WRF or Aladin, that runs in a nested mode. The outer grid, covering the North Atlantic and Europe, has a horizontal resolution of 0.2° ($\sim$ 22 km) and 31 layers in the vertical. The model is driven at the boundaries by the ECMWF model. It produces forecasts to +48 hour, four times a day. The inner grid, covering Northwest Europe, has a horizontal resolution of 0.1° ($\sim$ 11 km) and 40 layers in the vertical. It produces forecasts to +24 hour, eight times a day.

The difference between the downscaled wind and the NWP-model wind depends mainly on the difference in roughness and the wind speed, the influence of the PBL-height is of minor importance and it does not depend on forecasts time. So, it is sufficient to verify only the +03 hour Hirlam forecasts, provided every 3 hours during the verification period. Due to spin-up in the Hirlam model, which results in an underestimation of initialized wind speeds, these +03 hour model forecasts are used rather than the initialized analysis.

The NWP-model provides the 10-m wind and the PBL height at the NWP-grid points. The 10-m wind and PBL height are interpolated to the high resolution grid of the land-use map. This 10-m wind is used for comparison with the downscaled wind. The PBL height is calculated at the Hirlam points from the surface parameters and the model level parameters using the method of Vogelezang and Holtslag (1996). The PBL height is calculated on the input grid. As the depth of the boundary layer in the Netherlands usually is less than 3 km, the use of 10 layers of Hirlam data is sufficient.

6 Verification

The verification results of the 2L-model are presented for three test sites: coastal, land, and offshore (see Fig. 7). The first test location, "Hansweert", is located at a coastline in the Zeeland estuary. Hansweert is on the edge of a tidal waterway that is the main shipping route from the North Sea to the river Scheldt that provides access into the main land. This location was selected for its highly complex roughness map with large directional differences in roughness. The second location is the synoptic wind speed measurement site at Amsterdam Airport Schiphol (see Fig. 8 for details). This is a typical inland location with built-up areas. However, also at this site there are large directional differences in wind speed. The third location is the offshore site "Vlakte van de Raan". This site is entirely surrounded by water. The smallest distance from the Vlakte van de Raan to the coast of Zeeland is about 20 km. Results have been collected from several more test locations. However, the results for other locations are similar to those presented in this paper. The coastal and land locations are selected for the large differences in roughness as function of wind direction. At the offshore site there are no differences between the NWP-model roughness map and the local roughness map at this site, so the comparison of the NWP-model wind and the downscaled wind can be used to assess to effect of atmospheric stability on the downscaling.

For illustration purpose the impact of the local roughness on the wind in the PBL is demonstrated by comparing the results of 2L-model with the NWP-model winds. In Fig. 9(a) NWP-model wind at 10 m is plotted. The wind field, at a horizontal resolution of 0.1°, is interpolated bi-linearly to the 1 km resolution grid. In Fig. 9(b) the corresponding wind field produced by the 2L-model at a resolution of 1 km and at 10 m height is plotted. Note the abrupt changes in wind speed when the downscaled wind flow reaches the coast, whereas NWP-model winds change gradually near the coast. The downscaled winds over small water bodies can be more than 40% stronger than the NWP-model winds.

6.1 Observations

At the three test locations hourly observations were collected of the averaged wind speed and wind direction over the preceding ten-minute time interval. The measurement heights, relative to the station height, are 10 m at Schiphol airport and approximately 16.5 m at the measurement stations in Zeeland. The Zeeland measurements are corrected to the WMO standard height of 10 m. The reduction factor for the mean wind speed is based on a neutral logarithmic wind profile relation. The deviations of the corrected measurements from the wind speed at observation height are around 6% on average. The uncorrected measurements at 16.5-m height were not available to us in this period. In order to validate the downscaling model per wind sector, the observed wind direction was used to sample the data in 30°-intervals. Wind speeds less than 3 m s^{-1} were rejected in the verification analysis because for low wind speeds the wind direction is often variable.

A first verification data set has been collected in the period November 2001–February 2002. During this period, the daily averaged atmospheric stability changed from unstable-neutral in the beginning to strongly stable at the end. In the first months of the verification period (November–December 2001) the sea was significantly warmer than the land surface and the atmosphere. For the province of Zeeland this period was predominantly unstable over land and over water. In the second half of January 2002, the sea was much colder than the land surface and the atmosphere. A warm airflow in that period resulted in a strongly stable, stratified atmosphere. This data set has been collected to test the running scores of both the neutral and non-neutral implementation of the downscaling method. A second data set has been collected in the period October 2003–August 2004 for the same stations. This data set has been used to validate the downscaling method as function of wind direction.

6.2 Verification results

In the following results will be presented in terms of the mean error and the standard deviation of the error in the 10-m wind speed. The wind speed error is defined as

$$Error = Model - Observation,$$

where *Model* is the result of the Hirlam model or the downscaling method. The Hirlam model wind is interpolated bi-linearly to the observation location. The downscaled wind is the wind speed at the 500-m grid point nearest to the observation location. *Observation* stands for the measured mean wind speed over the preceding ten-minute time interval. The error statistics of the modeled wind direction are omitted in the presentation as those errors are

generally small. Wind direction errors in the NWP-model and in the local wind flow computed with the downscaling method are 10° on average.

6.2.1 Hansweert

Scatter plots of the modeled wind speed, computed by Hirlam and the 2L-model, versus the observed wind speed at location Hansweert are presented in Fig. 10. Fig. 10(a) shows that Hirlam underestimates the wind speed and the underestimation increases for stronger winds. Fig. 10(b) shows that the 2L-model leads to a major improvement of the surface wind. The downscaled wind estimates the measured wind speed better on average, the scatter is slightly reduced.

Fig. 11(a) and 11(b) show the 10-m wind speed error (30°-wide bins) of Hirlam and the 2L-model for the location Hansweert for the summer and winter period, respectively. At Hansweert Hirlam underestimates the surface wind speed when the wind direction is between 120° and 320°, and overestimates the wind speed for other wind directions. Fig. 6 shows that the underestimation (overestimation) corresponds to the directions where the Hirlam roughness is larger (smaller) than the local and regional roughness. The predominance of southern winds in the Netherlands results in the overall underestimation of the wind speed by Hirlam in Fig. 10(a).

In Fig. 12(a) the running scores for Hansweert are presented for the period November 2001–February 2002 (7-day averaging window). A large negative bias is found for Hirlam, increasing to -3 m s^{-1} during the stable period. The 2L-model method improves the surface wind for both periods with stable and unstable stratification: the bias is reduced significantly to an absolute value that is less than 0.5 m s^{-1} for the greater part of the verification period and for each wind direction.

6.2.2 Amsterdam Airport Schiphol

For location Amsterdam Airport Schiphol the verification results are presented in Figs. 11(c) and 11(d). The Hirlam bias is large for both the unstable and stable period (Fig. 12(b)) which shows that in general the Hirlam roughness that is used for Schiphol is too large. Variations in bias as a function of the wind direction are large. The maximum underestimation of the Hirlam surface wind occurs for southwesterly winds with a bias in the order of -3 m s^{-1} (30–40%). In this direction the footprint is over the runway and the roughness is very small. (cf. Fig. 8). For other wind directions, in which the wind mainly blows over built-up areas, the resulting Hirlam winds still underestimate the measured wind speed by 1 m s^{-1} on average.

As was already noted, the quality of the land-use map in the Schiphol area is poor: the concrete platforms of the airport are classified as built-up areas. As a result the regional roughness length for the 2L-model is generally too high as well and the 2L-model would underestimate the local wind speed, just like Hirlam. The 2L-model results in Figs. 11(c), 11(d) and 12(b) are achieved by using the local roughness for both the SL and the EL. Doing so the downscaling method improves the surface winds significantly. For the greater part of the verification period, and for most wind directions, the absolute value of the bias is less than 0.5 m s^{-1} in the summer period, and less than 1 m s^{-1} in the winter period.

6.2.3 Vlakte van de Raan

The verification scores for location 'Vlakte van de Raan' are presented in Figs. 11(e), 11(f), 12(d), and 12(c). In both Hirlam and the 2L-model the sea roughness is computed by application of the Charnock relation (Charnock, 1955; Garratt, 1977; Makin et al., 1995). The 2L-model replaces the Hirlam grid-box averaged surface roughness, which for the Vlakte van de Raan consists of sea roughness only, by the local roughness. As a result we may expect that at the Vlakte van de Raan the local wind computed by the 2L-model hardly differs from the grid-box averaged surface wind computed by Hirlam. This confirmed by Figs. 11(e) and 11(f). During summer as well as winter the mean error in the Hirlam surface wind, and consequently also in the downscaled surface wind, is less than 1 m s^{-1} for most wind directions.

Fig. 12(c) shows that the running scores of Hirlam and the 2L-model are identical as well. This figure proves that stability has little effect on the performance of the 2L-model. Both in stable and unstable conditions the negligence of stability effects in the upward transformation is counterbalanced in the downward transformation. This is a trivial result since in the same roughness length is used in the upward and downward transformation.

In Fig. 12(d) the running scores are plotted for the Hirlam forecast, and as derived after application of the non-neutral downscaling method. Here the Hirlam wind speed at the top of the PBL is used as input to the 2L-model and the stability, as derived from Hirlam, is taken into account in the transformation Eqs. 2 and 1. It is clear that the non-neutral downscaling method produces lower quality surface winds than Hirlam. Especially during the stable period, which starts in the second half of January 2002, the bias in the downscaled surface wind speed increases to almost 4 m s^{-1}. This large bias is caused by the stability corrections, since the Hirlam- and the 2L-model-roughness for this open-sea location is identical. During periods of neutral and unstable stratification (November–December 2001) the performance of the stability correction is better, but still slightly worse than the Hirlam per-

formance.

7 Conclusions

- The use of uniform, grid-box averaged, roughness information in NWP-models, to describe the local wind flow, leads to large errors in the representation of the wind in certain areas of the Netherlands.
- The 2L-model significantly reduces the mean error in the surface winds that are produced by Hirlam. The mean error in the modeled local wind speed is in absolute value less than 0.5 m s^{-1}, about 5–10% of the measured wind speeds, for most wind directions. For open-sea locations the 2L-model gives similar performance as Hirlam. The standard deviation of the error is only slightly reduced.
- The 2L-model gives an improved performance during neutral, unstable and stable atmospheric conditions. Errors due to not accounting for atmospheric stability in the 2L-model are counterbalanced by using an upward and subsequent downward transformation.
- A non-neutral implementation of the 2L-model suffers from stability correction problems that arise during stable stratification.
- Local and regional, wind direction dependent, roughness lengths can be derived from a land-use dataset by averaging surface roughness over the upstream area.
- The local roughness lengths compare well to those derived from gustiness analysis. This comparison reveals that the footprint length scale for the local roughness is about 0.6 km, which also sets the lower limit for the spatial resolution at which the downscaling method can be applied.
- The 2L-model is well capable of modeling the development of the wind speed after roughness transitions and gives similar results as internal boundary-layer models. The comparison confirms that the footprint length scale for the local roughness must be close to 0.6 km, and that the footprint length scale for the regional roughness is about 3 km.
- Inaccuracies in the land-use map may lead to biased downscaling results.

Acknowledgments

The presented downscaling method has been developed on the authority of the *Rijksdienst IJsselmeergebied*. Part of the research presented in this paper has been carried out within the framework of the projects Hydra and Nautilus, both supported by the Dutch National Water Board *Rijkswaterstaat*. The Hydra-project is supported by the *National Institute for Coastal and Marine*

Management (RIKZ) and the *Institute for Inland Water Management and Waste Water Treatment* (RIZA). Nautilus is supported by RIKZ.

The authors are grateful for the support and interest they received from the user group representatives of the Netherlands Ministry of Transport, Public works and Water management. Iwan Holleman and Vladimir Makin from the Royal Netherlands Meteorological Institute, and Bert Holtslag from Wageningen University and Research Centre, are acknowledged for commenting on the first draft of this paper. Jan-Rolf Hendriks from the Tidal Water Division in Zeeland is thanked for providing the wind observation data from the ZeGe measurement network.

References

Agterberg, R., Wieringa, J., 1989. Mesoscale terrain roughness mapping of the Netherlands. Tech. Rep. TR-115, Royal Netherlands Meteorological Institute.

Arya, S. P. S., 1977. Suggested revisions to certain boundary layer parameterization schemes used in atmospheric circulation models. Mon. Wea. Rev. 105, 215–227.

Baldauf, M., Fiedler, F., 2003. A parameterisation of the effective roughness length over inhomogeneous, flat terrain. Bound.-Layer Meteor. 106, 189–216.

Beljaars, A. C. M., 1987. On the memory of wind standard deviation for upstream roughness. Bound.-Layer Meteor. 38, 95–101.

Benschop, H., 1996. Windsnelheidsmetingen op zeestations en kust stations: herleiding waarden windsnelheid naar 10-meter niveau. Tech. Rep. TR-188, Royal Netherlands Meteorological Institute.

Bergström, H., Johansson, P.-E., Smedman, A.-S., 1988. A study of wind speed modification and internal boundary-layer heights in a coastal region. Bound.-Layer Meteor. 42, 313–335.

Bradley, E. F., 1968. A micrometeorological study of velocity profiles and surface drag in the region modified by a change in surface roughness. Quart. J. Roy. Meteor. Soc. 94, 361–379.

Brown, R. A., 1982. On two-layer models and the similarity functions for the PBL. Bound.-Layer Meteor. 24, 451–463.

Businger, J. A., Yaglom, A. M., 1971. Introduction to Obukhov's paper 'Turbulence in an atmosphere with a non-uniform temperature'. Bound.-Layer Meteor. 2, 3–6.

Charnock, H., 1955. Wind stress on a water surface. Quart. J. Roy. Meteor. Soc. 81, 639.

Claussen, M., 1990. Area-averaging of surface fluxes in a neutrally stratified,

horizontally inhomogeneous atmospheric boundary layer. Atmos. Environ. 24A, 1349–1360.

De Rooy, W. C., 1995. Regionalisation of meteorological parameters. Sc. Rep. WR95-06, Royal Netherlands Meteorological Institute.

De Rooy, W. C., Kok, K., 2002. On the use of physical and statistical downscaling techniques for NWP model output. Sc. Rep. WR2002-05, Royal Netherlands Meteorological Institute.

De Rooy, W. C., Kok, K., 2004. A combined physical-statistical approach for the downscaling of model wind speed. Wea. Forecasting 19, 485–495.

De Wit, A. J. W., Van der Heijden, T. G. C., Thunnissen, H. A. M., 1999. Vervaardiging en nauwkeurigheid van het LGN3 grondgebruiksbestand. DLO-Staring Centrum, Wageningen.

Duijm, N. J., 1983. Model voor de stroming in een neutrale oppervlakte laag na een verandering in oppervlakte ruwheid. Sc. Rep. WR 83-3, Royal Netherlands Meteorological Institute.

Frenzen, P., Vogel, C. A., 1995a. A further note "On the magnitude and apparent range of variation of the von Karman constant in the atmospheric surface layer". Bound.-Layer Meteor. 75, 315–317.

Frenzen, P., Vogel, C. A., 1995b. On the magnitude and apparent range of variation of the von Karman constant in the atmospheric surface layer. Bound.-Layer Meteor. 72, 371–392.

Garratt, J. R., 1977. Review of drag coefficients over oceans and continents. Mon. Wea. Rev. 105, 915–929.

Garratt, J. R., 1992. The Atmospheric Boundary Layer. Cambridge University Press, Cambridge.

Horst, T. W., 1999. The footprint for estimation of atmosphere-surface exchange fluxes by profile techniques. Bound.-Layer Meteor. 90, 171–188.

Horst, T. W., Weil, J. C., 1992. Footprint estimation for scalar flux measurements in the atmospheric surface layer. Bound.-Layer Meteor. 59, 279–296.

Horst, T. W., Weil, J. C., 1994. How far is far enough?: The fetch requirements for micrometeorological measurements of surface fluxes. J. Atmos. Oceanic Technol. 11, 1018–1025.

Hutjes, R. W. A., 1996. Transformation of near-surface meteorology in a small-scale landscape with forests and arable land. Ph.D. thesis, Rijksuniversiteit Groningen, the Netherlands.

Jackson, P. S., Hunt, J. C. R., 1975. Turbulent wind flow over a low hill. Quart. J. Roy. Meteor. Soc. 101, 929–955.

Jacobs, A. F. G., 1984. The flow around a thin closed fence. Bound.-Layer Meteor. 28, 317–328.

Jensen, N. O., 1978. Change of surface roughness and the planetary boundary layer. Quart. J. Roy. Meteor. Soc. 104, 351–356.

Kudryavtsev, V. N., Makin, V. K., Klein Tank, A. M. G., Verkaik, J. W., 2000. A model of wind transformation over water–land surfaces. Sc. Rep. WR-2000-01, Royal Netherlands Meteorological Institute.

Makin, V. K., 2003. Note on a parameterization of the sea drag. Bound.-Layer

Meteor. 106, 593–600.
Makin, V. K., Kudryavtsev, V. N., Mastenbroek, C., 1995. Drag of the sea surface. Bound.-Layer Meteor. 73, 159–182.
Mason, P. J., 1988. The formation of areally-averaged roughness lengths. Quart. J. Roy. Meteor. Soc. 114, 399–420.
Obukhov, A. M., 1971. Turbulence in an atmosphere with a non-uniform temperature. Bound.-Layer Meteor. 2, 7–29.
Onvlee, J. R. A., 1993. The performance of dragrelations in the WAQUA storm surge model. Tech. Rep. TR-149, Royal Netherlands Meteorological Institute.
Rao, K. S., Wyngaard, J. C., Coté, O. R., 1974. The structure of the two-dimensional internal boundary layer over a sudden change of surface roughness. J. Atmos. Sci. 31, 738–746.
Schmid, H. P., 1994. Source areas for scalars and scalar fluxes. Bound.-Layer Meteor. 67, 293–318.
Schmid, H. P., Bünzli, D., 1995. The influence of surface texture on the effective roughness length. Quart. J. Roy. Meteor. Soc. 121, 1–21.
Sozzi, R., Favaron, M., Georgiadis, T., 1998. Method for estimation of surface roughness and similarity function of wind speed vertical profile. J. Appl. Meteor. 37, 461–469.
Taylor, P. A., 1987. Comments and further analysis on effective roughness lengths for use in numerical models. Bound.-Layer Meteor. 39, 403–418.
Tennekes, H., 1973. The logarithmic wind profile. J. Atmos. Sci. 30, 234–238.
Townsend, A. A., 1965. The response of a turbulent boundary layer to abrupt changes in surface conditions. J. Fluid Mech. 22, 799–822.
Troen, I., Petersen, E. L., 1989. European Wind Atlas. Risø National Laboratory, Roskilde, Denmark.
Undén, P., Rontu, L., Jarvinen, H., Lynch, P., Calvo, J., Cats, G., Cuxart, J., K.Eerola, Fortelius, C., Garcia-Moya, J. A., Jones, C., Lenderink, G., McDonald, A., McGrath, R., Navascues, B., Nielsen, N. W., Odegaard, V., Rodriguez, E., Rummukainen, M., Room, R., Sattler, K., Savijarvi, H., Sass, B. H., Schreur, B., The, H., Tijm, S., 2002. Hirlam-5 scientific documentation. Tech. rep., SMHI.
Van Wijk, A. J. M., Beljaars, A. C. M., Holtslag, A. A. M., Turkenburg, W. C., 1990. Diabatic wind speed profiles in coastal regions: comparison of an internal boundary layer (IBL) model with observations. Bound.-Layer Meteor. 51, 49–74.
Verkaik, J. W., 2000. Evaluation of two gustiness models for exposure correction calculations. J. Appl. Meteor. 39, 1613–1626.
Verkaik, J. W., Smits, A., 2001. Interpretation and estimation of the local wind climate. In: Proceedings of the 3rd European and African conference on wind engineering. 2–6 July, 2001, Eindhoven, the Netherlands, pp. 43–56.
Vogelezang, D., Holtslag, A., 1996. Evaluation and model impacts of alternative boundary-layer height formulations. Bound.-Layer Meteor. 81, 245–269.
Wieringa, J., 1976. An objective exposure correction method for average wind

speeds measured at a sheltered location. Quart. J. Roy. Meteor. Soc. 102, 241–253.

Wieringa, J., 1980. A revaluation of the kansas mast influence on measurements of stress and cup anemometer overspeeding. Bound.-Layer Meteor. 18, 411–430.

Wieringa, J., 1986. Roughness-dependent geographical interpolation of surface wind speed averages. Quart. J. Roy. Meteor. Soc. 112, 867–889.

Wieringa, J., 1993. Representative roughness parameters for homogeneous terrain. Bound.-Layer Meteor. 63, 323–363.

Wyngaard, J. C., Businger, J. A., Kaimal, J. C., Larsen, S. E., 1982. Comments on 'A revaluation of the Kansas mast influence on measurements of stress and cup anemometer overspeeding'. Bound.-Layer Meteor. 22, 245–250.

Table 1. Land-use classes in LGN3+ and the assigned roughness lengths.

ID	Class Name	z_0 (m)
0	no data	0.03
1	grass	0.03
2	maize	0.17
3	potatoes	0.07
4	beets	0.1
5	cereals	0.16
6	other agricultural crops	0.04
8	greenhouses	0.1
9	orchards	0.39
10	bulb cultivation	0.1
11	deciduous forest	0.75
12	coniferous forest	0.75
16	fresh water	0.001
17	salt water	0.001
18	continuous urban area	1.6
19	built-up in rural area	0.5
20	deciduous forest in urban area	1.1
21	coniferous forest in urban area	1.1
22	built-up area with dense forest	2.
23	grass in built-up area	0.03
24	bare soil in built-up area	0.001
25	main roads and railways	0.1
26	buildings in rural area	0.5
27	runways	0.0003
28	parking lots	0.1

30	salt marshes	0.0002
31	beaches and dunes	0.0003
32	sparsely vegetated dunes	0.06
33	vegetated dunes	0.02
34	heath lands in dune areas	0.03
35	shifting sands	0.0003
36	heath lands	0.03
37	heath lands with minor grass influence	0.04
38	heath lands with major grass influence	0.06
39	raised bogs	0.06
40	forest in raised bogs	0.75
41	miscellaneous swamp vegetation	0.03
42	reed swamp	0.1
43	forest in swamp areas	0.75
44	swampy pastures in peat areas	0.07
45	herbaceous vegetation	0.03
46	bare soil in natural areas	0.001

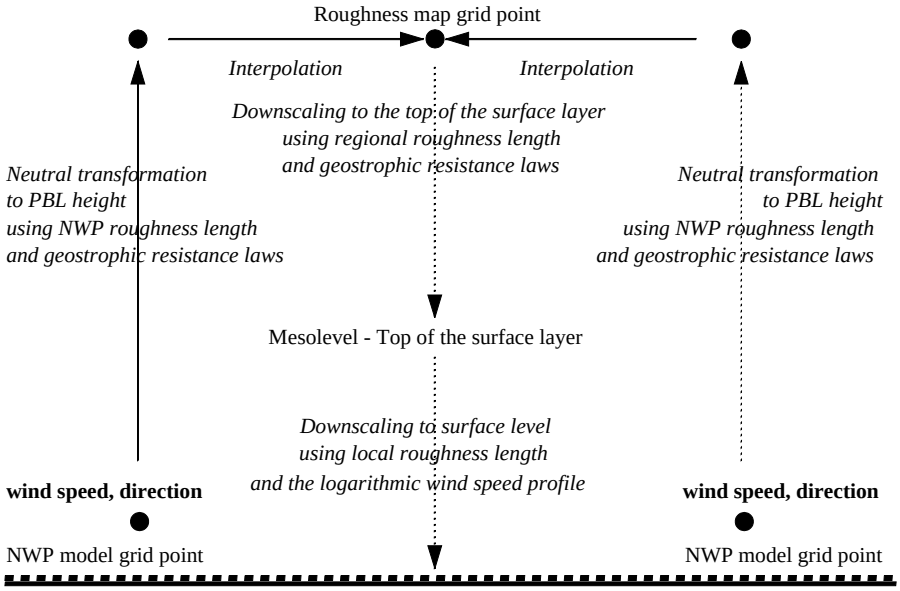

Fig. 1. Schematic diagram of the downscaling method.

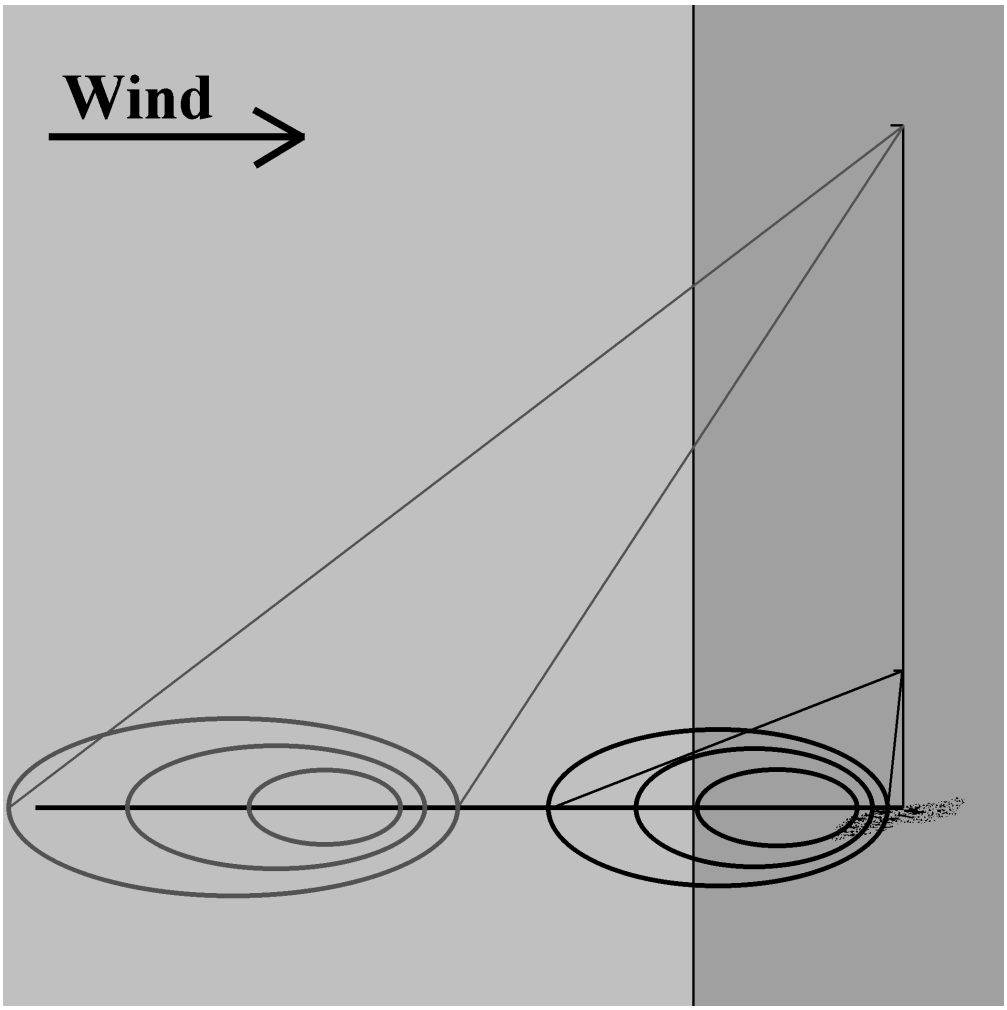

Fig. 2. Illustration of the footprint for two different measuring heights near a coastline. All numbers and scale ratios in this example are fictitious.

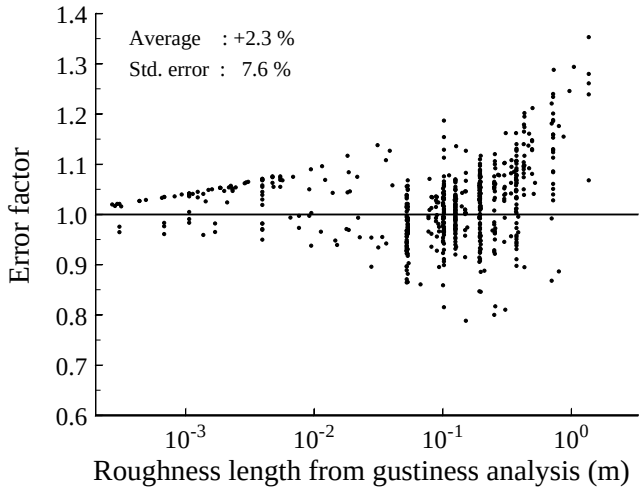

Fig. 3. Comparison of the roughness lengths derived from gustiness to those from the footprint model and the roughness map. An error factor larger than 1 implies that the gustiness roughness is larger than the footprint roughness.

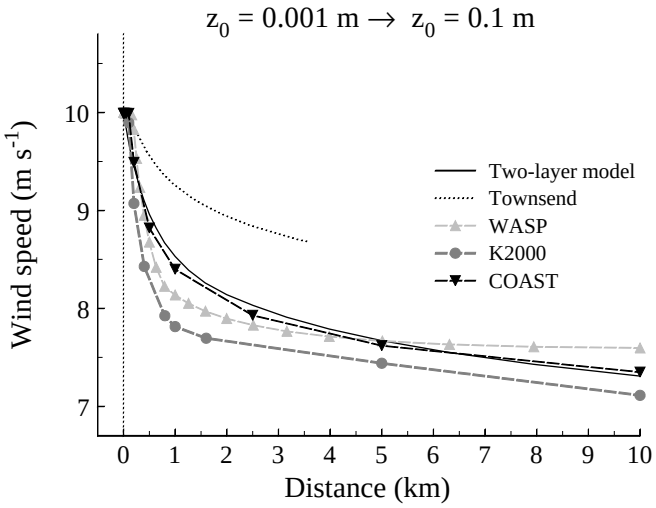

(a) Smooth-to-rough transition.

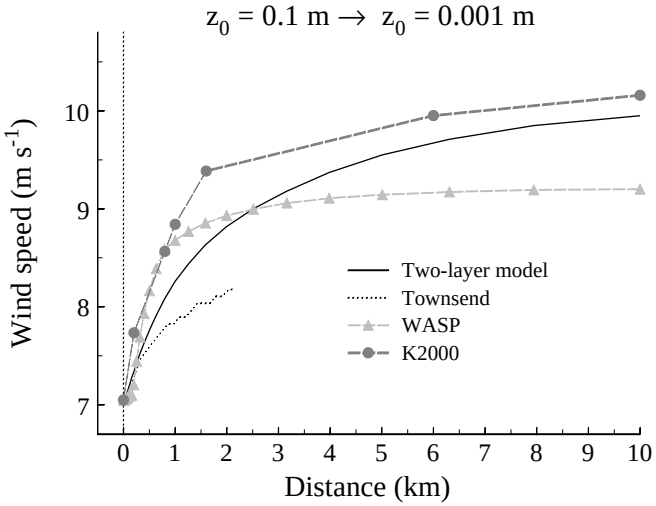

(b) Rough-to-smooth transition.

Fig. 4. The development of the wind speed in the 2L-model compared with several IBL-models: the surface-layer IBL-model by Townsend (1965); the Wind atlas analysis and application programme Troen et al. (1989, WASP); the analytical IBL-model of the full PBL by Kudryavtsev et al. (2000, K2000); the surface-layer IBL-model by Van Wijk et al. (1990, COAST).

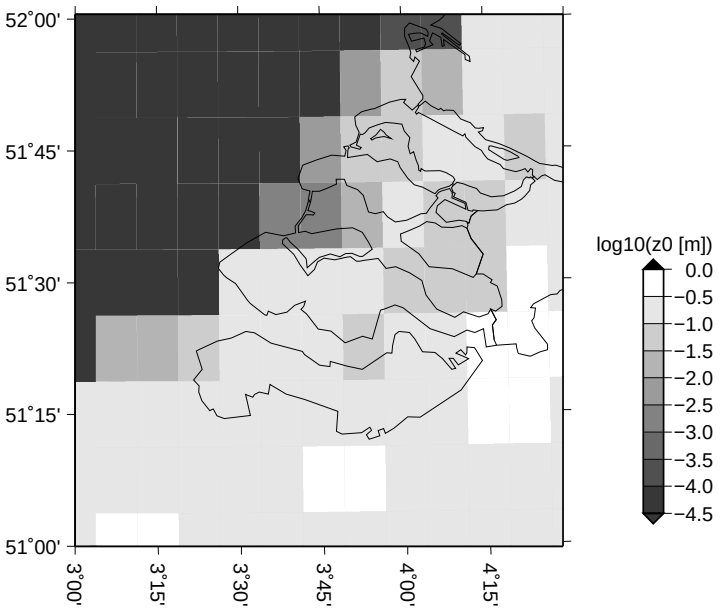

(a) NWP-model roughness map.

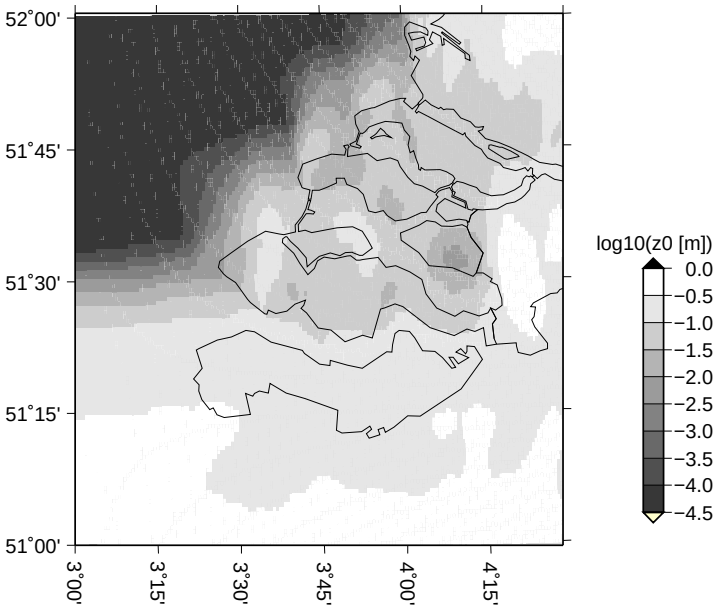

(b) Local roughness map.

Fig. 5. Roughness maps of the Zeeland estuaries. The resolution of the NWP-model roughness map is 0.1°. The resolution of the local roughness map is 0.5 km. The local roughness map is derived for a homogeneous wind field (5 m s^{-1} southwest).

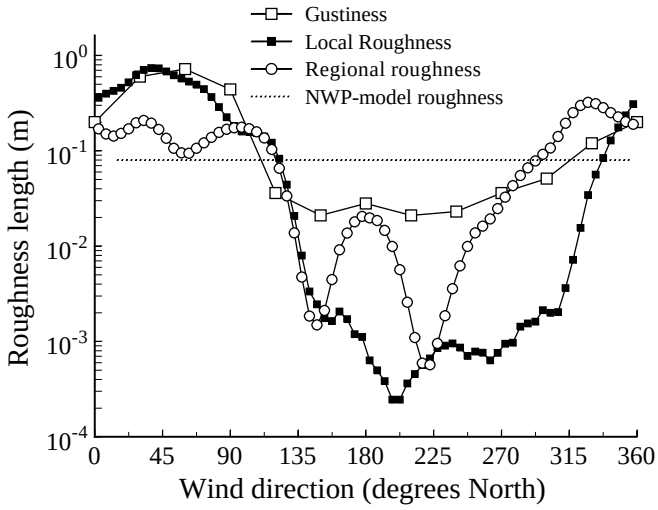

Fig. 6. Roughness lengths at test location Hansweert. The gustiness derived roughness is compared to the local roughness, the regional roughness, and the (directionally constant) NWP-model grid scale roughness.

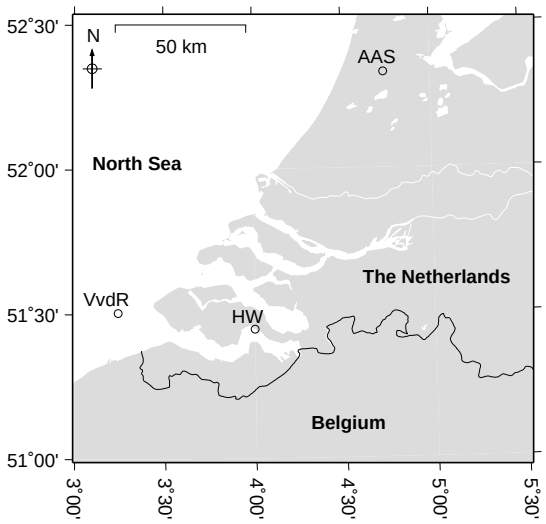

Fig. 7. Map of the south-west part of The Netherlands. The test locations are encircled. The offshore site 'VvdR' indicates the site 'Vlakte van de Raan', inland 'AAS' indicates 'Amsterdam Airport Schiphol', and in the Zeeland estuaries 'HW' indicates 'Hansweert'.

Fig. 8. Map of the take-off and touchdown area at Schiphol airport. The size of map is about 10×8 km^2. The arrow marks the synoptic wind measurement location used for validation.

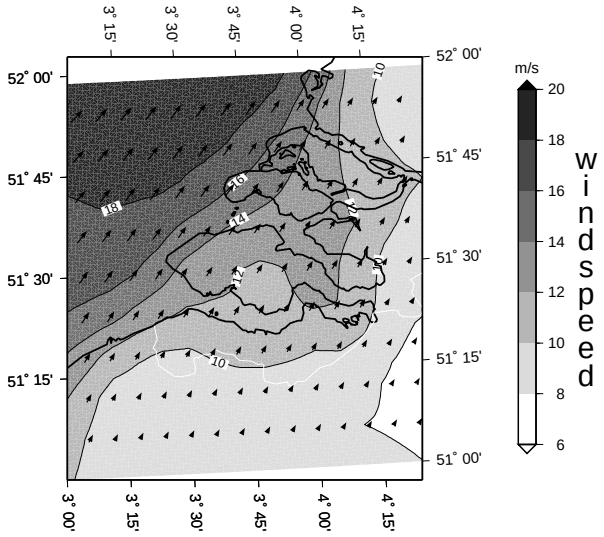

(a) NWP-model surface wind.

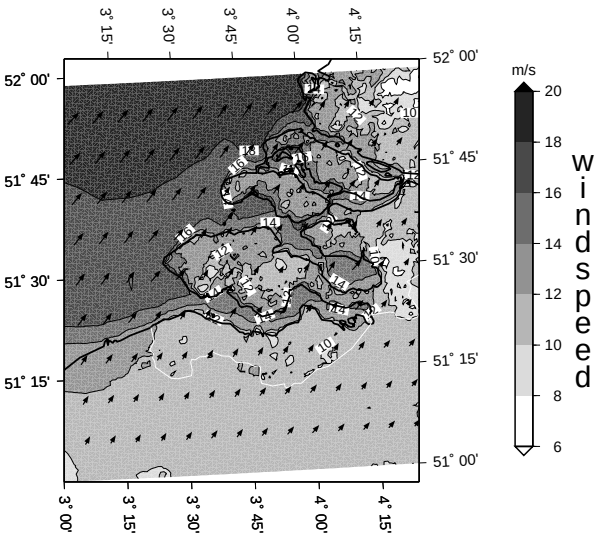

(b) Downscaled surface wind. The southern part of the map covers Belgium. We do not have land-use data for Belgium. A dummy value for the roughness is used here. Consequently the downscaled wind speed over Belgium is uniform.

Fig. 9. Wind field at 10-m height for Zeeland valid for February 2002, 22nd 00h UTC. The color scale indicates the wind speed, the arrows indicate the wind direction. The prevailing wind direction is southwest.

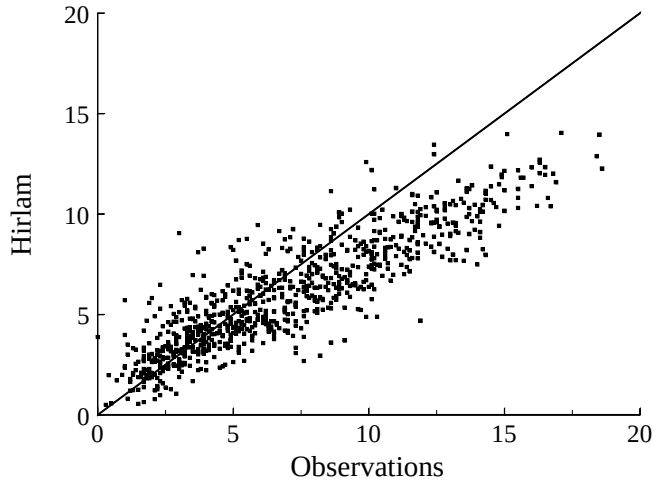

(a) Hirlam model wind speed versus in situ observations.

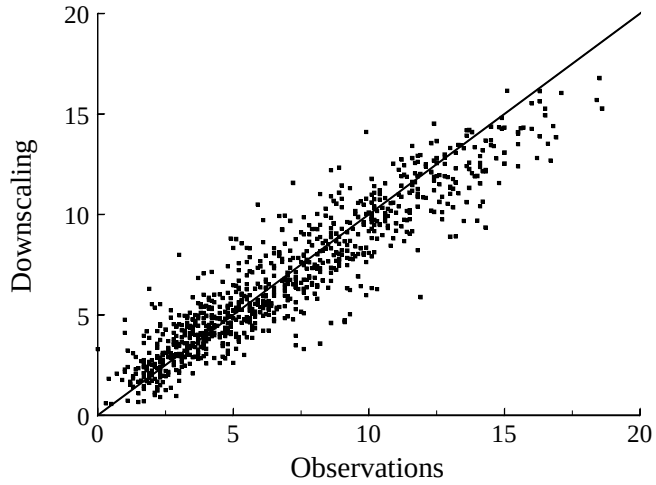

(b) Downscaled wind speed versus in situ observations.

Fig. 10. Scatter plot +3-hour forecast of the Hirlam model wind and the downscaled wind versus the observed wind speed at Hansweert.

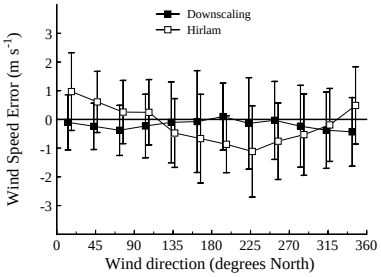

(a) Summer period at Hansweert.

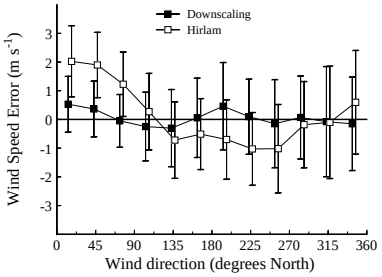

(b) Winter period at Hansweert.

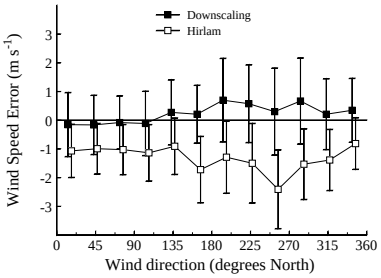

(c) Summer period at Amsterdam Airport Schiphol.

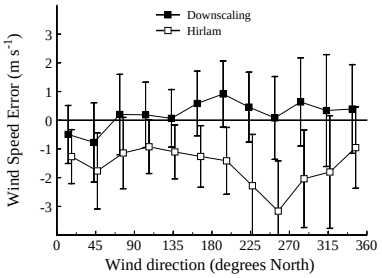

(d) Winter period at Amsterdam Airport Schiphol.

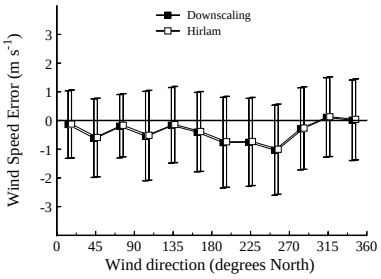

(e) Summer period at Vlakte van de Raan.

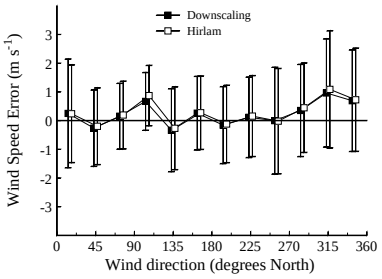

(f) Winter period at Vlakte van de Raan.

Fig. 11. Mean and standard deviation of the wind speed error of the +3-hour forecast of the NWP-model and the downscaling method in the winter period October 2003–March 2004 and the summer period April 2004–August 2004.

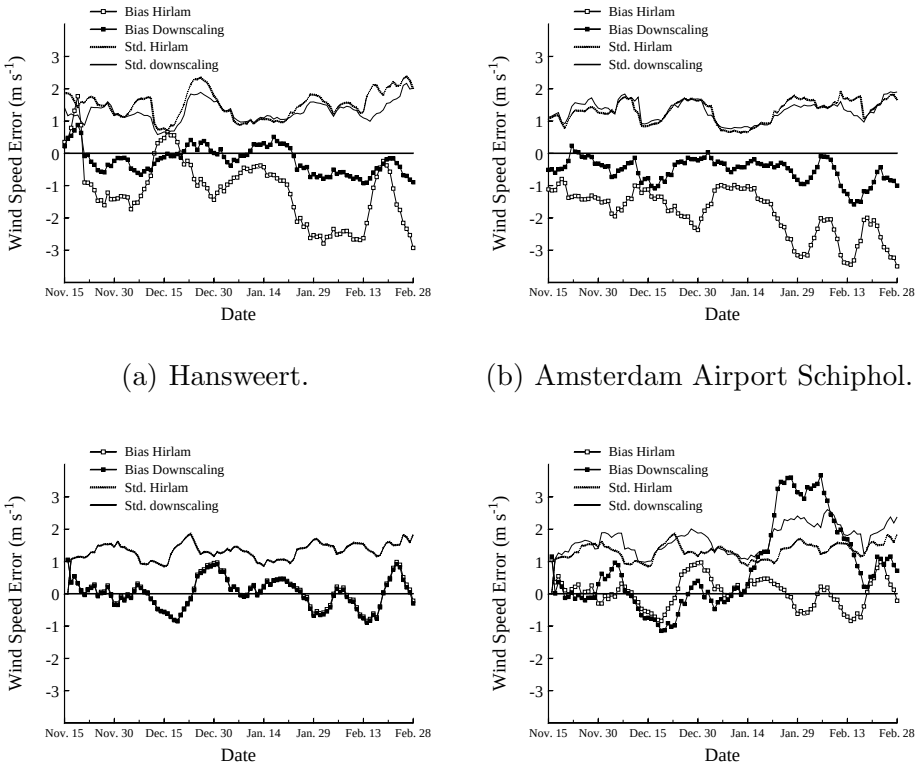

(a) Hansweert.

(b) Amsterdam Airport Schiphol.

(c) Vlakte van de Raan.

(d) Non-neutral downscaling method at Vlakte van de Raan.

Fig. 12. Running mean and standard deviation (7-day averaging period) of the wind speed error of the +3-hour forecast of the Hirlam model and the downscaling method in the period November 2001–February 2002.